Immunity, Volume *56*

Supplemental information

Tissue resident iNKT17 cells facilitate cancer cell extravasation in liver metastasis via interleukin-22

Anastasios D. Giannou, Jan Kempski, Ahmad Mustafa Shiri, Jöran Lücke, Tao Zhang, Lilan Zhao, Dimitra E. Zazara, Filippo Cortesi, Kristoffer Riecken, Maria Carolina Amezcua Vesely, Jun Siong Low, Hao Xu, Eleanna Kaffe, Laura Garcia-Perez, Theodora Agalioti, Yoshito Yamada, Wolfgang Jungraithmayr, Ehud Zigmond, Karl-Frederick Karstens, Babett Steglich, Jonas Wagner, Leonie Konczalla, Antonella Carambia, Kornelius Schulze, Johann von Felden, Peter May, Daria Briukhovetska, Tanja Bedke, Leonie Brockmann, Sarah Starzonek, Tobias Lange, Claudia Koch, Sabine Riethdorf, Penelope Pelczar, Marius Böttcher, Morsal Sabihi, Francis J. Huber, Matthias Reeh, Julia Kristin Grass, Ramez Wahib, Hannes Seese, Björn-Ole Stüben, Mohammad Fard-Aghaie, Anna Duprée, Pasquale Scognamiglio, Gabriel Plitzko, Jan Meiners, Shiwa Soukou, Agnes Wittek, Caroline Manthey, Ioannis C. Maroulis, Petra C. Arck, Daniel Perez, Bin Gao, Sotirios G. Zarogiannis, Till Strowig, Renata Pasqualini, Wadih Arap, Javier Suárez Gosálvez, Sebastian Kobold, Immo Prinz, Andreas H. Guse, Michael Tachezy, Tarik Ghadban, Asmus Heumann, Jun Li, Nathaniel Melling, Oliver Mann, Jakob R. Izbicki, Klaus Pantel, Udo Schumacher, Ansgar W. Lohse, Richard A. Flavell, Nicola Gagliani, and Samuel Huber

SUPPLEMENTAL INFORMATION

Tissue resident iNKT17 cells facilitate cancer cell extravasation in liver metastasis via IL-22

Anastasios D. Giannou, Jan Kempski, Ahmad Mustafa Shiri, Jöran Lücke, Tao Zhang, Lilan Zhao, Dimitra E. Zazara, Filippo Cortesi, Kristoffer Riecken, Maria Carolina Amezcua Vesely, Jun Siong Low, Hao Xu, Eleanna Kaffe, Laura Garcia-Perez, Theodora Agalioti, Yoshito Yamada, Wolfgang Jungraithmayr, Ehud Zigmond, Karl-Frederick Karstens, Babett Steglich, Jonas Wagner, Leonie Konczalla, Antonella Carambia, Kornelius Schulze, Johann von Felden, Peter May, Daria Briukhovetska, Tanja Bedke, Leonie Brockmann, Sarah Starzonek, Tobias Lange, Claudia Koch, Sabine Riethdorf, Penelope Pelczar, Marius Böttcher, Morsal Sabihi, Francis J. Huber, Matthias Reeh, Julia Kristin Graß, Ramez Wahib, Hannes Seese, Ole Stüben, Mohammad Fard-Aghaie, Anna Duprée, Pasquale Scognamiglio, Gabriel Plitzko, Jan Meiners, Shiwa Soukou, Agnes Wittek, Caroline Manthey, Ioannis C. Maroulis, Petra C. Arck, Daniel Perez, Bin Gao, Sotirios G. Zarogiannis, Till Strowig, Renata Pasqualini, Wadih Arap, Javier Suárez Gosálvez, Sebastian Kobold, Immo Prinz, Andreas H. Guse, Michael Tachezy, Tarik Ghadban, Asmus Heumann, Jun Li, Nathaniel Melling, Oliver Mann, Jakob R. Izbicki, Klaus Pantel, Udo Schumacher, Ansgar W. Lohse, Richard A. Flavell, Nicola Gagliani, and Samuel Huber

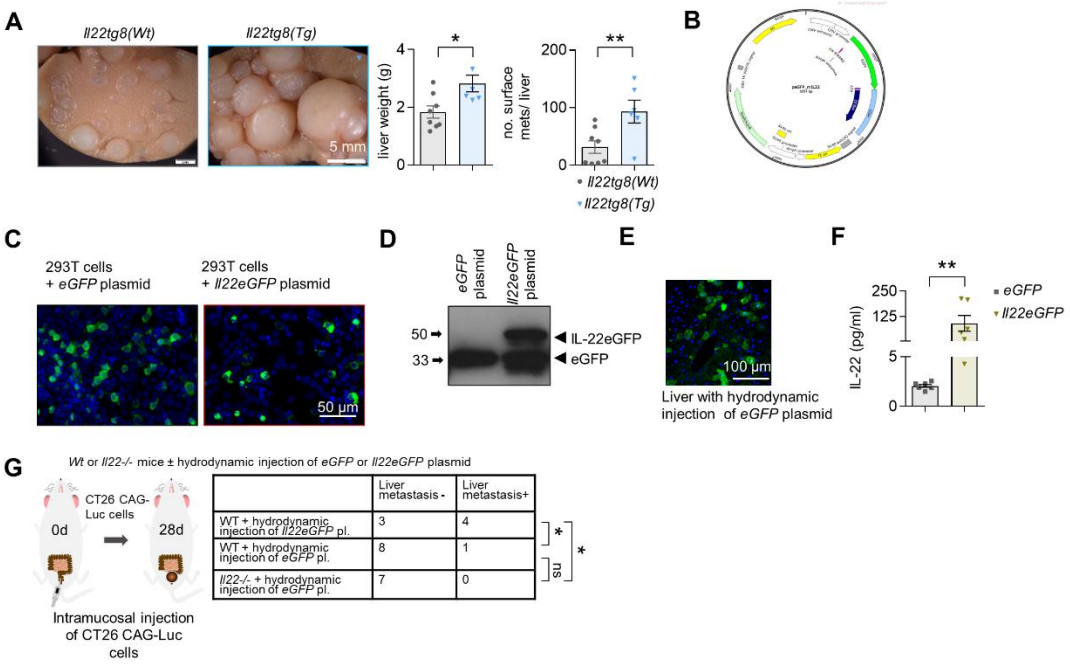

	Liver metastasis -	Liver metastasis+	
WT + hydrodynamic injection of *Il22eGFP* pl.	3	4	*
WT + hydrodynamic injection of *eGFP* pl.	8	1	ns
Il22-/- + hydrodynamic injection of *eGFP* pl.	7	0	*

Figure S1, related to Figure 1. High IL-22 levels promote liver metastasis

(A) Representative pictures, liver weight and number of macroscopic metastases in total liver of mice with normal (*Il22tg8*$^{(Wt)}$) or high (*Il22tg8*$^{(Tg)}$) levels of IL-22. n ≥ 5 mice per group. Scale bar: 5 mm. (B) Map of *Il22eGFP* plasmid. (C) *In vitro* cultured 293T cells transfected with *eGFP* (left) and *Il22eGFP* (right) plasmid. Scale bar: 50µm. (D) 293T cells were transfected with *peGFP* and *pIl22eGFP* plasmid. GFP levels were measured using immunoblotting. (E) Representative picture of liver tissue upon hydrodynamic injection of *peGFP* plasmid. Scale bar: 100µm. (F) IL-22 serum levels in mice hydrodynamically injected with *eGFP* or *Il22eGFP* plasmid. n ≥ 6 mice per group. (G) Schematic overview and incidence of liver metastases in mice with no (*Il22-/-* mice upon hydrodynamic injection of eGFP plasmid), normal (WT upon hydrodynamic injection of eGFP plasmid) or high (WT upon hydrodynamic injection of Il22eGFP plasmid) levels of IL-22 using hydrodynamic overexpression of eGFP or Il22eGFP plasmid and intramucosal injection of CT26 CAG-Luc cells. n ≥ 7 mice per group. Data presented as mean ± SEM. ns>0.05; *:p<0.05; **:p≤0.01; ***:p≤0.001 as assessed by Mann-Whitney U test (A, F) or Fischer´ s exact test (G).

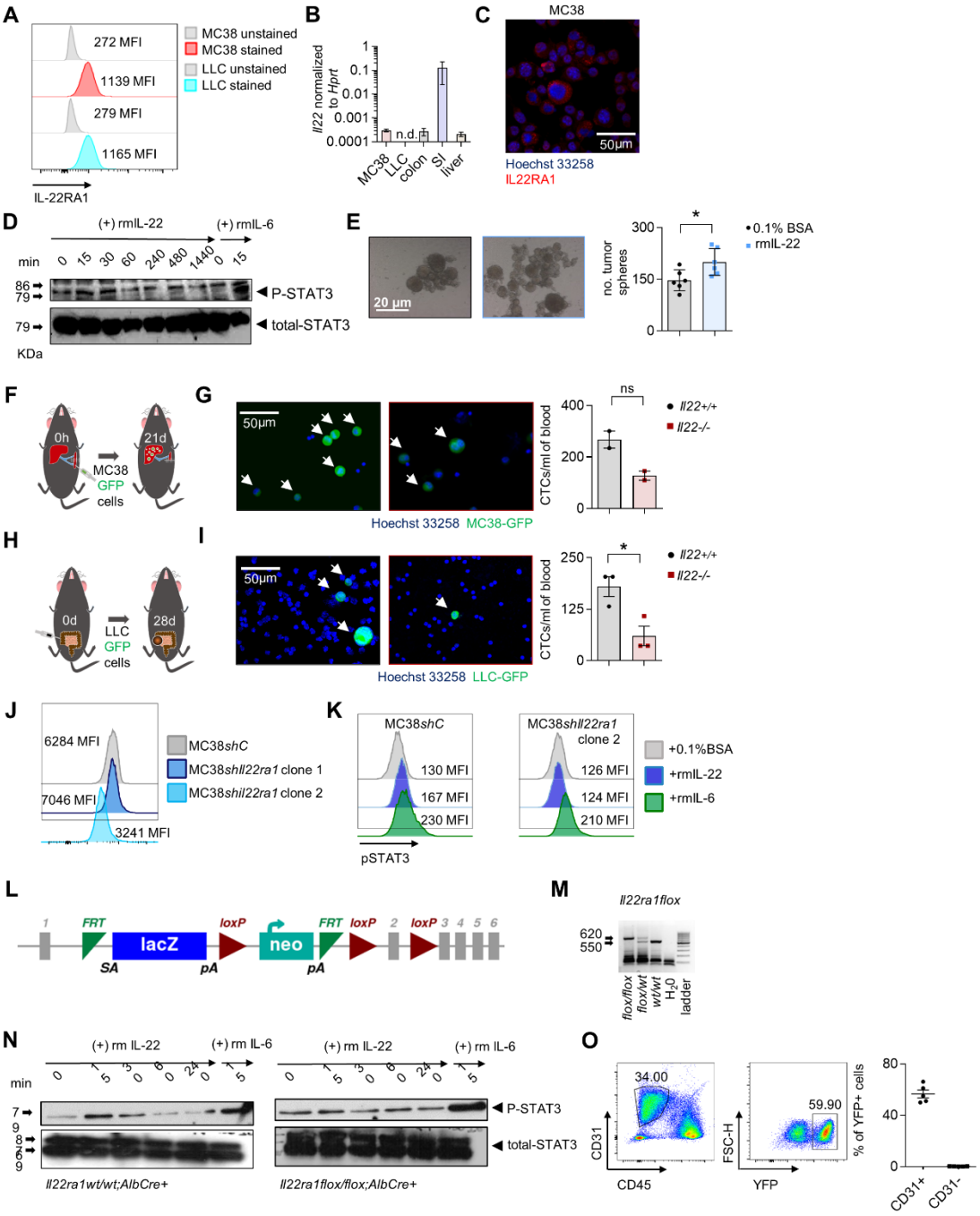
A
272 MFI
1139 MFI
279 MFI
1165 MFI
MC38 unstained
MC38 stained
LLC unstained
LLC stained
IL-22RA1
B
Il22 normalized to Hprt
n.d
MC38
LLC
colon
SI
liver
C
MC38
50µm
Hoechst 33258
IL22RA1
D
(+) rmIL-22
(+) rmIL-6
min
0 15 30 60 240 480 1440 0 15
86
79
P-STAT3
79
total-STAT3
KDa
E
20 µm
no. tumor spheres
0.1% BSA
rmIL-22
F
0h
21d
MC38 GFP cells
G
50µm
Hoechst 33258 MC38-GFP
CTCs/ml of blood
ns
Il22+/+
Il22-/-
H
0d
28d
LLC GFP cells
I
50µm
Hoechst 33258 LLC-GFP
CTCs/ml of blood
Il22+/+
Il22-/-
J
6284 MFI
7046 MFI
3241 MFI
MC38shC
MC38shIl22ra1 clone 1
MC38shil22ra1 clone 2
K
MC38shC
130 MFI
167 MFI
230 MFI
MC38shIl22ra1 clone 2
126 MFI
124 MFI
210 MFI
+0.1%BSA
+rmIL-22
+rmIL-6
pSTAT3
L
1
FRT
lacZ
loxP
neo
FRT
loxP
2
loxP
3 4 5 6
SA
pA
pA
M
Il22ra1flox
620
550
flox/flox
flox/wt
wt/wt
H2O
ladder
N
(+) rm IL-22
(+) rm IL-6
(+) rm IL-22
(+) rm IL-6
min
0 1 5 30 60 240 0 1 5
0 1 5 30 60 240 0 1 5
7
9
8
6
9
P-STAT3
total-STAT3
Il22ra1wt/wt;AlbCre+
Il22ra1flox/flox;AlbCre+
O
34.00
CD31
CD45
59.90
FSC-H
YFP
% of YFP+ cells
CD31+
CD31-

Figure S2, related to Figure 2. IL-22 signaling increases cancer cell stemness

(A) IL-22RA1 surface protein levels in MC38 and LLC cancer cells measured using FACS (B) *Il22* mRNA levels in MC38, LLC cancer cells as well as murine colon, small intestine (SI) and liver (RNA extracts from total tissue). (C) Immunostaining of IL-22RA1 in MC38 cells. Scale bar: 50µm. (D) Immunoblotting of p-STAT3 on MC38 cells upon IL-22 exposure in different time points. (E) Representative pictures and number of tumor spheres after exposure to 0.1% BSA or rmIL-22. Scale bar: 20 µm. (F) Schematic overview of intrasplenic injection of MC38 GFP-labelled cells for forced liver metastasis induction. (G) Representative pictures and number of GFP-labelled CTCs in $Il22^{+/+}$ and $Il22^{-/-}$ mice. n=2 independent experiments with 5 mice per group each time. Scale bar: 50 µm. (H) Schematic overview of cecum injection of LLC-GFP cells for spontaneous liver metastasis induction in $Il22^{+/+}$ and $Il22^{-/-}$ mice (I) Representative pictures and number of GFP-labelled CTCs in $Il22^{+/+}$ and $Il22^{-/-}$ mice. n=3 independent experiments with 6 mice per group each time. Scale bar: 50 µm. (J) Validation of silencing of *Il22ra1* in MC38 cancer cells by FACS. (K) Functional assay of silencing of *Il22ra1* in MC38 cancer cells by analyzing the pSTAT3 levels upon IL-22 exposure. (L) Construct map of $Il22ra1^{flox/flox}$ mice. (M) Genotyping PCR of $Il22ra1^{-/-}$ and $Il22ra1^{flox/flox}$ mice. (N) Hepatocytes were isolated from $Il22ra1^{wt/wt};Alb^{Cre+}$ and $Il22ra1^{flox/flox};Alb^{Cre+}$ mice and treated with 50 ng/ml recombinant murine (rm) IL-22 for 15 min, 30 min, 60 min and 240 min. IL-6 was used as a positive control. pSTAT3 levels were measured using immunoblotting. n=2 mice per group. (O) Gating strategy for identification of YFP+ LSECs isolated from liver of $Il22ra1^{flox/flox};Cdh5^{Cre+}$ mice and respective quantification. Data presented as mean ± SEM. ns:p>0.05; *:p<0.05; **:p≤0.01; ***:p≤0.001 as assessed by Mann-Whitney U test (E, G).

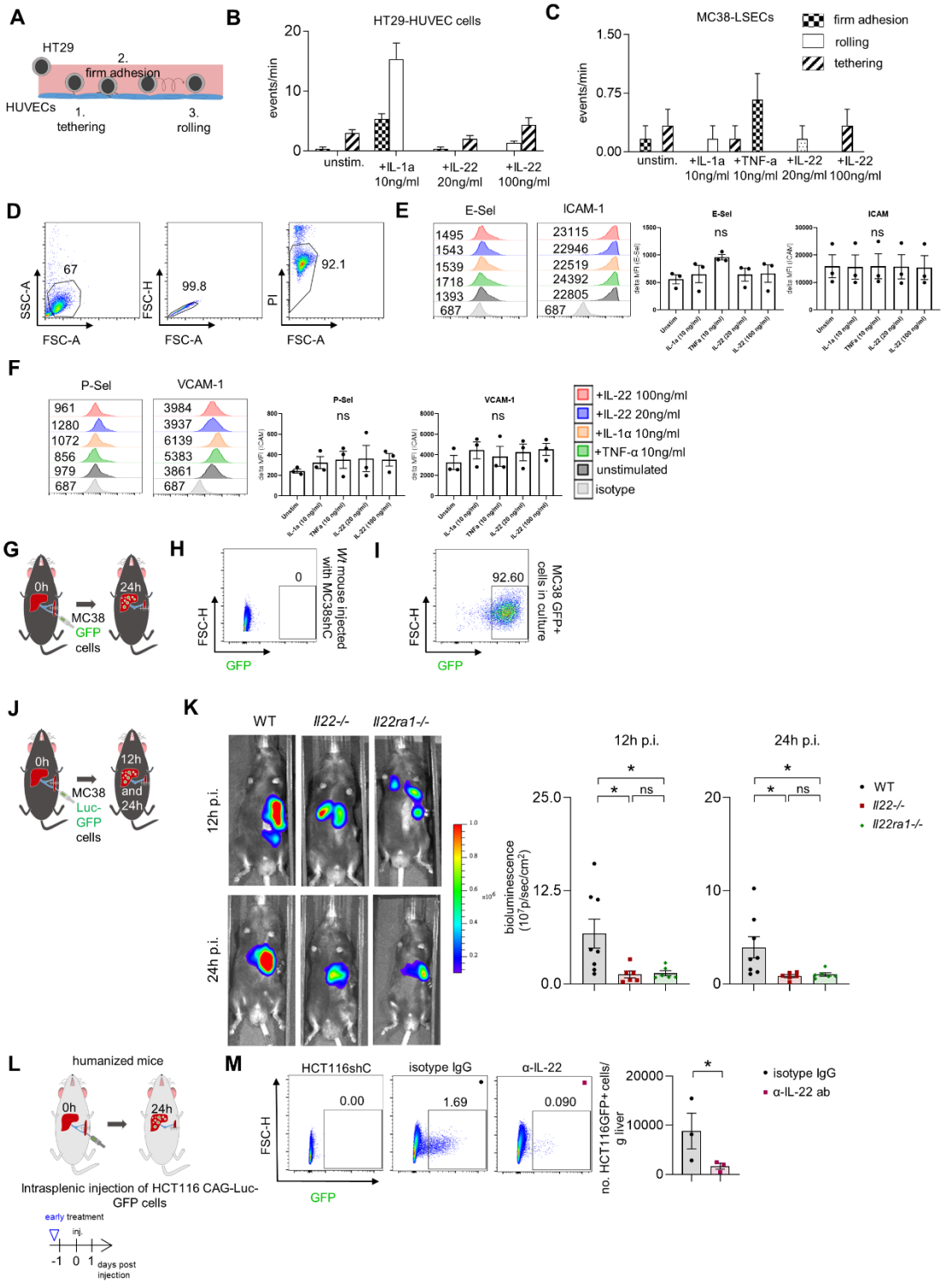
A
HT29
2.
firm adhesion
HUVECs
1.
tethering
3.
rolling
B
HT29-HUVEC cells
events/min
unstim.
+IL-1a 10ng/ml
+IL-22 20ng/ml
+IL-22 100ng/ml
C
MC38-LSECs
firm adhesion
rolling
tethering
events/min
unstim.
+IL-1a 10ng/ml
+TNF-a 10ng/ml
+IL-22 20ng/ml
+IL-22 100ng/ml
D
SSC-A
FSC-A
67
FSC-H
99.8
PI
92.1
E
E-Sel
ICAM-1
1495
1543
1539
1718
1393
687
23115
22946
22519
24392
22805
687
ns
F
P-Sel
VCAM-1
961
1280
1072
856
979
687
3984
3937
6139
5383
3861
687
+IL-22 100ng/ml
+IL-22 20ng/ml
+IL-1α 10ng/ml
+TNF-α 10ng/ml
unstimulated
isotype
G
0h
24h
MC38 GFP cells
H
0
FSC-H
GFP
Wt mouse injected with MC38shC
I
92.60
FSC-H
GFP
MC38 GFP+ cells in culture
J
0h
12h and 24h
MC38 Luc-GFP cells
K
WT
Il22-/-
Il22ra1-/-
12h p.i.
24h p.i.
bioluminescence (10^7 p/sec/cm^2)
WT
Il22-/-
Il22ra1-/-
L
humanized mice
0h
24h
Intrasplenic injection of HCT116 CAG-Luc-GFP cells
early treatment
inj.
-1 0 1 days post injection
M
HCT116shC
isotype IgG
α-IL-22
0.00
1.69
0.090
FSC-H
GFP
no. HCT116GFP+ cells/ g liver
isotype IgG
α-IL-22 ab

Figure S3, related to Figure 3. IL-22 does not affect cancer cell endothelial adhesion, but cancer cell extravasation

(A) Schematic overview of the *in vitro* adhesion assay of endothelial HUVEC and HT-29 cancer cells. (B) HT-29 cancer cells were perfused over HUVEC cells (flow rate 8 mL/h) and retaining cells were counted. (C) MC38 cancer cells were perfused over LSECs (flow rate 8 mL/h) and retaining cells were counted. (D-F) FACS plots and histograms showing the expression of adhesion molecules, namely E-Sel, P-Sel, ICAM-1, VCAM-1, on LSECs upon stimulation with TNF-α, IL-1α and IL-22 in two different concentrations. (G) Schematic overview of intrasplenic injection of MC38 GFP-labelled cells in WT mice (extravasation assay). (H) FACS plot of liver of Wt mouse after intrasplenic injection of MC38 shC cells (I) FACS plot of MC38 GFP-labelled cells in culture. (J) Schematic overview of intrasplenic injection of MC38 Luc-GFP-labelled cells in WT, *Il22*$^{-/-}$ and *Il22ra1*$^{-/-}$ mice (extravasation assay). (K) Bioluminescent imaging and quantification of bioluminescent signal of WT, *Il22*$^{-/-}$ and *Il22ra1*$^{-/-}$ mice 12 and 24 hours after intrasplenic injection of MC38 Luc-GFP cells. Bioluminescent scale: $1x10^5$-$1x10^6$ photons/sec/cm^2/sr. (L) Injection of HCT116 CAG-Luc-GFP-labelled cells in humanized mice receiving a treatment with Fezakinumab (a human α-IL-22 antibody) or IgG control antibody. (M) Representative FACS plots showing the percentage of extravasated GFP+ cancer cells in the liver and bar plots showing the total number of extravasated cancer cells from (L). Data presented as mean ± SEM. ns>0.05; *:p<0.05; **:p≤0.01 as assessed by one-way ANOVA with Bonferroni post hoc tests (B, C, E, F and K) or Mann-Whitney U test (M).

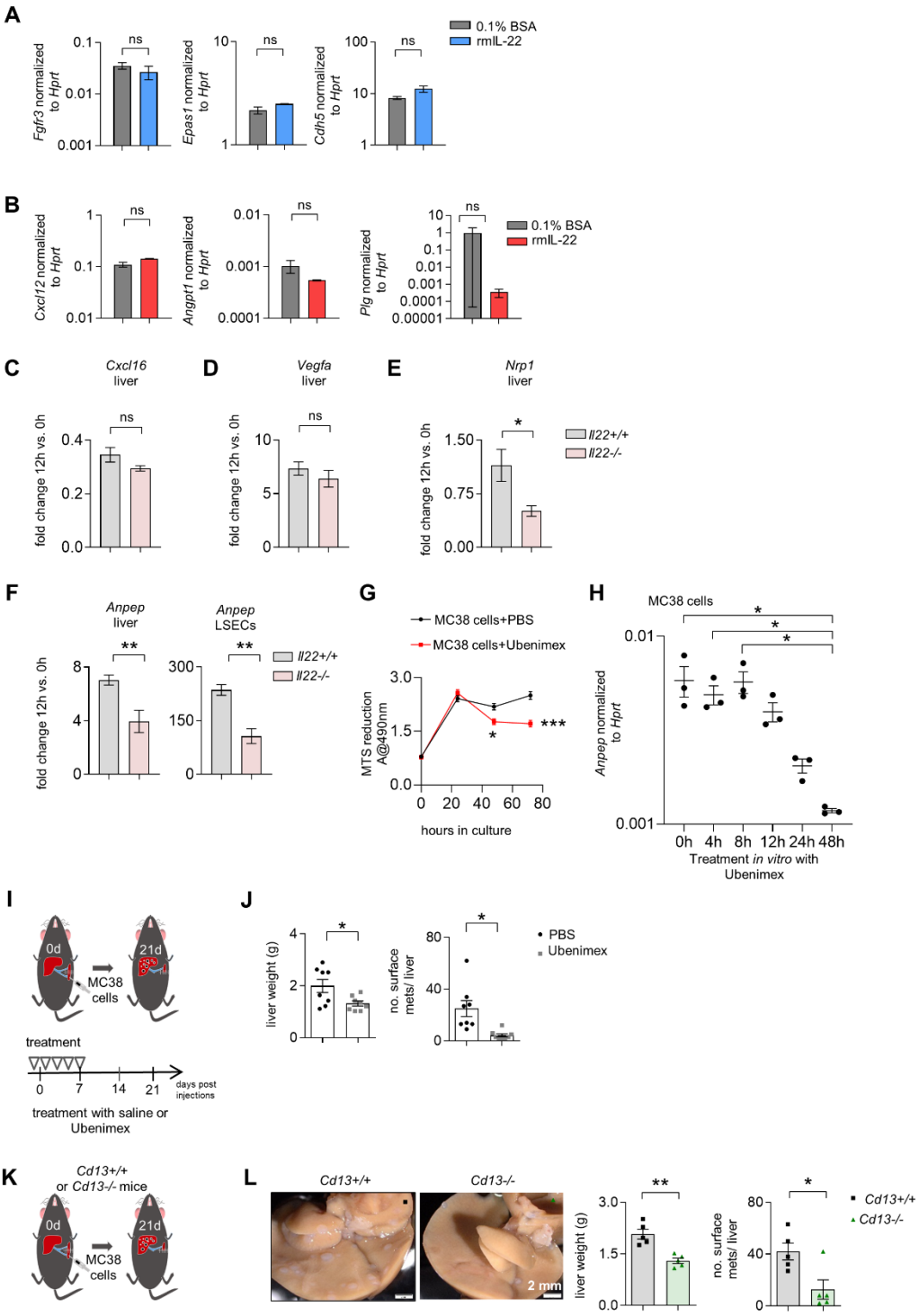
A
Fgfr3 normalized to Hprt
Epas1 normalized to Hprt
Cdh5 normalized to Hprt
ns
0.1% BSA
rmIL-22
B
Cxcl12 normalized to Hprt
Angpt1 normalized to Hprt
Plg normalized to Hprt
C
Cxcl16 liver
D
Vegfa liver
E
Nrp1 liver
fold change 12h vs. 0h
Il22+/+
Il22-/-
F
Anpep liver
Anpep LSECs
G
MC38 cells+PBS
MC38 cells+Ubenimex
MTS reduction A@490nm
hours in culture
H
MC38 cells
Anpep normalized to Hprt
Treatment in vitro with Ubenimex
I
0d
21d
MC38 cells
treatment
days post injections
treatment with saline or Ubenimex
J
liver weight (g)
no. surface mets/ liver
PBS
Ubenimex
K
Cd13+/+ or Cd13-/- mice
L
Cd13+/+
Cd13-/-
2 mm

Figure S4, related to Figure 4. Inhibition of aminopeptidases reduces liver metastasis formation

(A) *Fgfr3, Epas1* and *Cdh5* expression in LSECs upon stimulation with rmIL-22**.** (B) *Cxcl12, Angpt1,* and *Plg* expression in LSECs upon stimulation with rmIL-22**.** (C, D, E) Fold change of C*xcl16, Vegfa* and *Nrp1* expression in the liver tissue 12h post intrasplenic injection of MC38 cells in *Il22*$^{+/+}$ and *Il22*$^{-/-}$ mice compared to 0h. (F) Fold change of *Anpep* expression in LSECs and liver tissue 12h post intrasplenic injection of MC38 cells in WT and *Il22*$^{-/-}$ mice (G) MTS assay of MC38 cells upon Ubenimex treatment in different time points of culture. (H) *Anpep* expression of MC38 cells upon Ubenimex treatment in different time points of culture. (I) Schematic overview of intrasplenic injection of MC38 cells for forced liver metastasis induction in mice receiving a control or Ubenimex treatment, respectively. (J) Liver weight and number of macroscopic metastases in total liver of mice treated with PBS or Ubenimex. n ≥ 8 mice per group. (K) Schematic overview of intrasplenic injection of MC38 cells for forced liver metastasis induction in *Cd13*$^{+/+}$ and *Cd13*$^{-/-}$ mice. (L) Representative pictures, number of macroscopic metastases in total liver and liver weight of *Cd13*$^{+/+}$ mice compared to *Cd13*$^{-/-}$ mice. n = 5 mice per group. Data presented as mean ± SEM. ns>0.05; *:p<0.05; **:p≤0.01 as assessed by one-way (H, K, L) or two-way ANOVA with Bonferroni post hoc tests (G) or Mann-Whitney U test (A-F, J).

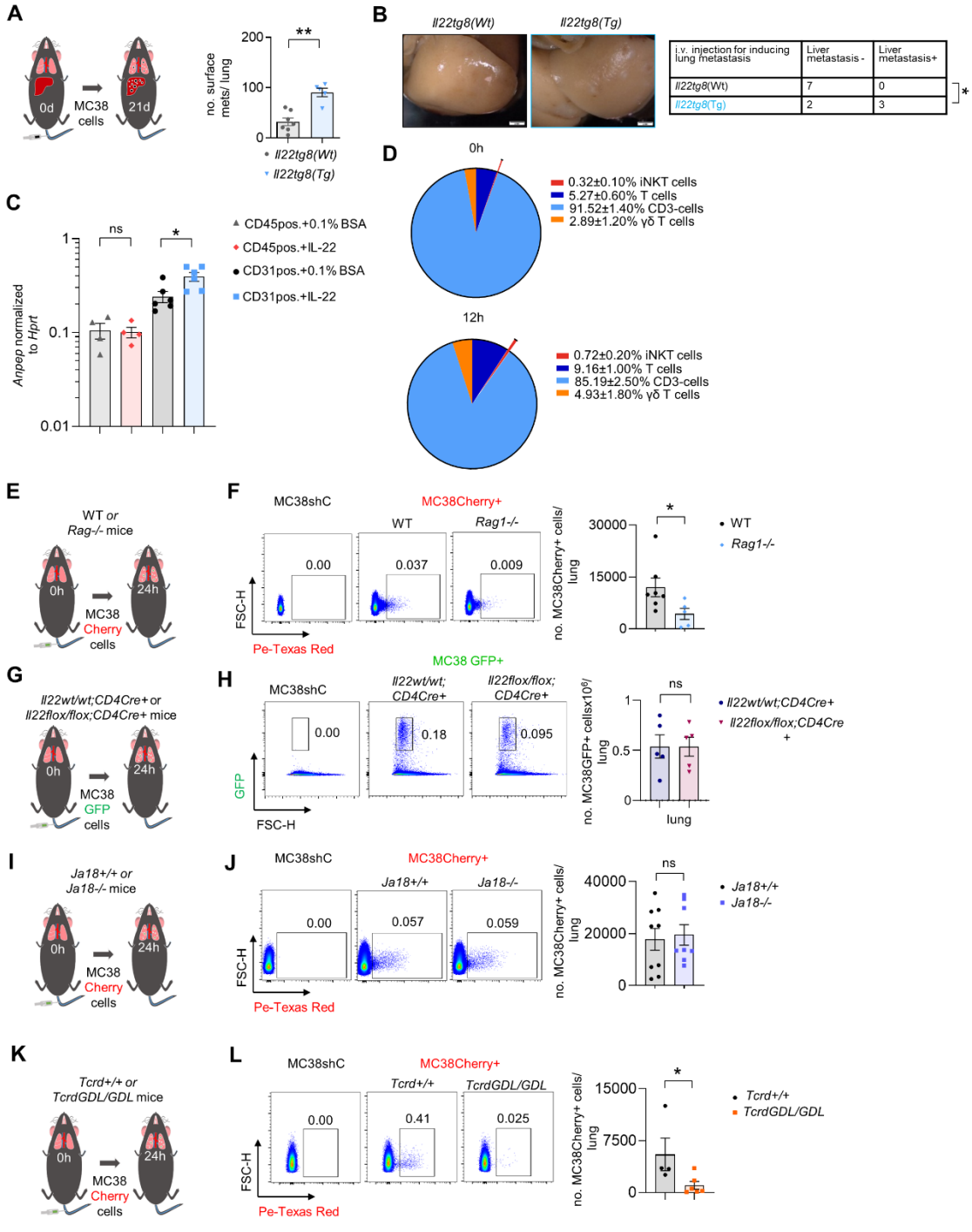
A
0d
MC38 cells
21d
no. surface mets/ lung
200
100
0
**
Il22tg8(Wt)
Il22tg8(Tg)
B
Il22tg8(Wt)
Il22tg8(Tg)
i.v. injection for inducing lung metastasis
Liver metastasis -
Liver metastasis+
Il22tg8(Wt)
7
0
Il22tg8(Tg)
2
3
*
C
ns
*
1
0.1
0.01
Anpep normalized to Hprt
CD45pos.+0.1% BSA
CD45pos.+IL-22
CD31pos.+0.1% BSA
CD31pos.+IL-22
D
0h
0.32±0.10% iNKT cells
5.27±0.60% T cells
91.52±1.40% CD3-cells
2.89±1.20% γδ T cells
12h
0.72±0.20% iNKT cells
9.16±1.00% T cells
85.19±2.50% CD3-cells
4.93±1.80% γδ T cells
E
WT or Rag-/- mice
0h
24h
MC38 Cherry cells
F
MC38shC
MC38Cherry+
WT
Rag1-/-
0.00
0.037
0.009
FSC-H
Pe-Texas Red
no. MC38Cherry+ cells/ lung
30000
15000
0
*
WT
Rag1-/-
G
Il22wt/wt;CD4Cre+ or Il22flox/flox;CD4Cre+ mice
0h
24h
MC38 GFP cells
H
MC38shC
MC38 GFP+
Il22wt/wt; CD4Cre+
Il22flox/flox; CD4Cre+
0.00
0.18
0.095
GFP
FSC-H
no. MC38GFP+ cellsx10⁶/ lung
1
0.5
0
ns
lung
Il22wt/wt;CD4Cre+
Il22flox/flox;CD4Cre+
I
Ja18+/+ or Ja18-/- mice
0h
24h
MC38 Cherry cells
J
MC38shC
MC38Cherry+
Ja18+/+
Ja18-/-
0.00
0.057
0.059
FSC-H
Pe-Texas Red
no. MC38Cherry+ cells/ lung
40000
20000
0
ns
Ja18+/+
Ja18-/-
K
Tcrd+/+ or TcrdGDL/GDL mice
0h
24h
MC38 Cherry cells
L
MC38shC
MC38Cherry+
Tcrd+/+
TcrdGDL/GDL
0.00
0.41
0.025
FSC-H
Pe-Texas Red
no. MC38Cherry+ cells/ lung
15000
7500
0
*
Tcrd+/+
TcrdGDL/GDL

Figure S5, related to Figure 5. IL-22 producing γδ T cells affect cancer cell extravasation into the lung via ANPEP induction

(A) Schematic overview of intravenous injection of MC38 cells for forced lung metastasis induction and number of macroscopic metastases in total lungs of mice with normal (*Il22tg8*$^{(Wt)}$) or high (*Il22tg8*$^{(Tg)}$) levels of IL-22. n ≥ 5 mice per group. (B) Representative pictures and percentage of mice with normal (*Il22tg8*$^{(Wt)}$) or high (*Il22tg8*$^{(Tg)}$) levels of IL-22 which develop macroscopic liver metastases. n ≥ 5 mice per group. (C) *Anpep* expression of sorted CD45+ and CD31+ cells upon stimulation with rmIL-22 (100 ng/µl). (D) Diagram showing the proportion of different immune subtypes of CD45+IL-22+ cells in murine lung 0 and 12 hours upon intravenous injection of MC38 cells. (E) Schematic overview of intravenous injection of MC38 Cherry-labelled cells in WT and *Rag1*$^{-/-}$ mice. (F) Representative FACS plots and statistics of MC38 Cherry-labelled extravasated cells in Wt and *Rag1*$^{-/-}$ mice. n ≥ 4 mice per group. (G) Schematic overview of intravenous injection of MC38 GFP-labelled cells in *Il22*$^{wt/wt}$*;CD4*$^{Cre+}$ and *Il22*$^{flox/flox}$*;CD4*$^{Cre+}$ mice (extravasation assay). n ≥ 5 mice per group. (H) Representative FACS plots and number of extravasated cancer cells from *Il22*$^{wt/wt}$*;CD4*$^{Cre+}$ and *Il22*$^{flox/flox}$*;CD4*$^{Cre+}$ mice 24h post intravenous injection. n ≥ 4 mice per group (I) Schematic overview of intravenous injection of MC38 Cherry-labelled cells in *Ja18*$^{+/+}$ and *Ja18*$^{-/-}$ mice. n ≥ 8 mice per group. (J) Representative FACS plots and number of extravasated cancer cells from *Ja18*$^{+/+}$ or *Ja18*$^{-/-}$ mice 24h post intravenous injection. Mice were sacrificed and the number of extravasated cancer cells in the lungs was quantified. (K) Schematic overview of intravenous injection of MC38 Cherry-labelled cells in *Tcrd*$^{GDL/GDL}$ and *Tcrd*$^{+/+}$ mice following DT (Diphtheria toxin) injection (DT injection in *Tcrd*$^{GDL/GDL}$ mice leads to γδ T cell depletion). n ≥ 4 mice per group. (L) Representative FACS plots and number of extravasated cancer cells from *Tcrd*$^{GDL/GDL}$ or *Tcrd*$^{+/+}$ mice 24h post intravenous injection. Mice were sacrificed and the number of extravasated cancer cells in the lungs were quantified. Data presented as mean ± SEM. ns>0.05; *:p<0.05; **:p≤0.01; ***:p≤0.001 as assessed by Mann-Whitney U test (C, F, H, J and L) or Fischer´ s exact test (B).

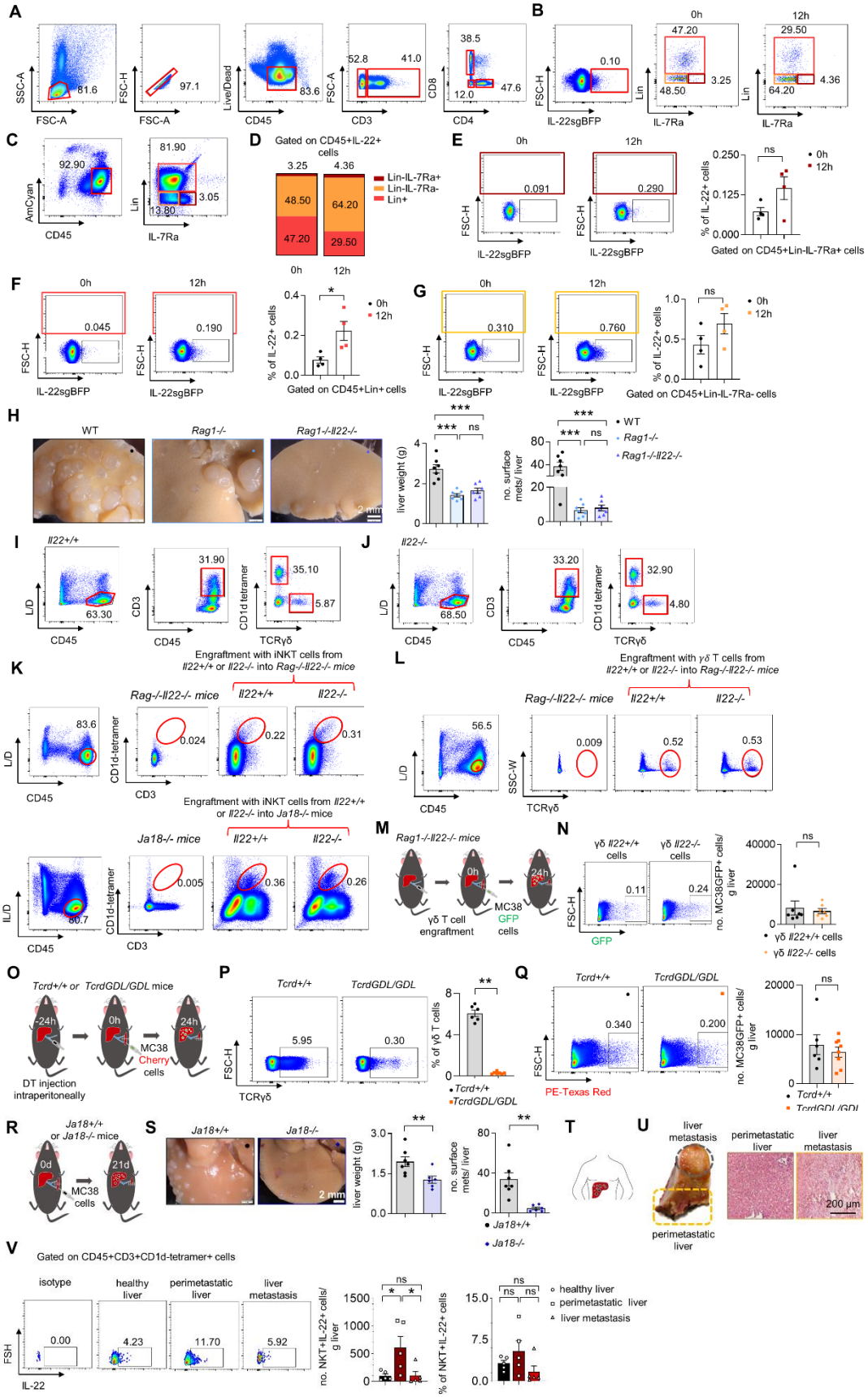
A
SSC-A
FSC-A
81.6
FSC-H
FSC-A
97.1
Live/Dead
CD45
83.6
FSC-A
CD3
52.8
41.0
CD8
CD4
38.5
12.0
47.6
B
0h
12h
FSC-H
IL-22sgBFP
0.10
Lin
IL-7Ra
47.20
48.50
3.25
29.50
64.20
4.36
C
AmCyan
CD45
92.90
Lin
IL-7Ra
81.90
3.05
13.80
D
Gated on CD45+IL-22+ cells
3.25
4.36
48.50
64.20
47.20
29.50
Lin-IL-7Ra+
Lin-IL-7Ra-
Lin+
0h
12h
E
0h
12h
FSC-H
IL-22sgBFP
0.091
0.290
% of IL-22+ cells
ns
0h
12h
Gated on CD45+Lin-IL-7Ra+ cells
F
0h
12h
FSC-H
IL-22sgBFP
0.045
0.190
% of IL-22+ cells
*
Gated on CD45+Lin+ cells
G
0h
12h
FSC-H
IL-22sgBFP
0.310
0.760
% of IL-22+ cells
ns
Gated on CD45+Lin-IL-7Ra- cells
H
WT
Rag1-/-
Rag1-/-Il22-/-
2 mm
liver weight (g)
***
ns
no. surface mets/ liver
WT
Rag1-/-
Rag1-/-Il22-/-
I
Il22+/+
L/D
CD45
63.30
CD3
31.90
CD1d tetramer
35.10
5.87
TCRγδ
J
Il22-/-
L/D
CD45
68.50
CD3
33.20
CD1d tetramer
32.90
4.80
TCRγδ
K
Engraftment with iNKT cells from Il22+/+ or Il22-/- into Rag-/-Il22-/- mice
Rag-/-Il22-/- mice
Il22+/+
Il22-/-
L/D
CD45
83.6
CD1d-tetramer
CD3
0.024
0.22
0.31
Engraftment with iNKT cells from Il22+/+ or Il22-/- into Ja18-/- mice
Ja18-/- mice
Il22+/+
Il22-/-
IL/D
CD45
60.7
CD1d-tetramer
CD3
0.005
0.36
0.26
L
Engraftment with γδ T cells from Il22+/+ or Il22-/- into Rag-/-Il22-/- mice
Rag-/-Il22-/- mice
Il22+/+
Il22-/-
L/D
CD45
56.5
SSC-W
TCRγδ
0.009
0.52
0.53
M
Rag1-/-Il22-/- mice
0h
24h
γδ T cell engraftment
MC38 GFP cells
N
γδ Il22+/+ cells
γδ Il22-/- cells
FSC-H
GFP
0.11
0.24
no. MC38GFP+ cells/ g liver
ns
γδ Il22+/+ cells
γδ Il22-/- cells
O
Tcrd+/+ or TcrdGDL/GDL mice
-24h
0h
24h
DT injection intraperitoneally
MC38 Cherry cells
P
Tcrd+/+
TcrdGDL/GDL
FSC-H
TCRγδ
5.95
0.30
% of γδ T cells
**
Tcrd+/+
TcrdGDL/GDL
Q
Tcrd+/+
TcrdGDL/GDL
FSC-H
PE-Texas Red
0.340
0.200
no. MC38GFP+ cells/ g liver
ns
Tcrd+/+
TcrdGDL/GDL
R
Ja18+/+ or Ja18-/- mice
0d
21d
MC38 cells
S
Ja18+/+
Ja18-/-
2 mm
liver weight (g)
**
no. surface mets/ liver
**
Ja18+/+
Ja18-/-
T
U
liver metastasis
perimetastatic liver
perimetastatic liver
liver metastasis
200 μm
V
Gated on CD45+CD3+CD1d-tetramer+ cells
isotype
healthy liver
perimetastatic liver
liver metastasis
FSH
IL-22
0.00
4.23
11.70
5.92
no. NKT+IL-22+ cells/ g liver
ns
% of NKT+IL-22+ cells
ns
healthy liver
perimetastatic liver
liver metastasis

Figure S6, related to Figure 6. IL-22 producing iNKT cells, but not T, γδ T and Lin- cells, affect cancer cell extravasation into the liver parenchyma (A) Gating strategy used to assess the IL-22 expression in different immune subtypes upon intrasplenic injection of MC38 cells. (B) Gating strategy used to assess the Lin-IL-7Ra+IL-22+, Lin-IL-7Ra-IL-22+ and Lin+IL-22+ cells isolated from murine liver 0 and 12h upon intrasplenic injection of MC38 cells. (C) Gating strategy used to assess the Lin-IL-7Ra+, Lin-IL-7Ra- and Lin+ cells isolated from murine liver 0 and 12h after intrasplenic injection of MC38 cells. (D) Diagram showing the proportion of different subtypes of CD45+IL-22+ cells in murine liver 0 and 12h after intrasplenic injection of MC38 cells. (E, F, G) FACS plots showing the production of IL-22 in the Lin-IL-7Ra+, Lin-IL-7Ra- and Lin+ cells isolated from murine liver 0 and 12h after intrasplenic injection of MC38 cells. n ≥ 4 mice per group. (H) Liver weight and number of macroscopic liver metastases post intrasplenic injection of MC38 cells in WT, *Rag*$^{-/-}$ *and Rag*$^{-/-}$*;Il22*$^{-/-}$ mice. n ≥ 6 mice per group. (I, J) FACS plots showing the gating strategy used for the sorting of iNKT and γδ T cells from *Il22*$^{+/+}$ and *Il22*$^{-/-}$ mice. (K) Engraftment with iNKT cells (total population) from *Il22*$^{+/+}$ or *Il22*$^{-/-}$ into *Rag1*$^{-/-}$ and *Ja18*$^{-/-}$ mice. (L) Engraftment with γδ T cells from *Il22*$^{+/+}$ into *Rag1*$^{-/-}$*Il22*$^{-/-}$ mice. (M) Schematic overview of intrasplenic injection of MC38 GFP-labelled cells in *Rag*$^{-/-}$*Il22*$^{-/-}$ mice engrafted with *Il22*$^{+/+}$or *Il22*$^{-/-}$ γδ T cells (extravasation assay). (N) Representative FACS plots and number of extravasated cancer cells from *Rag*$^{-/-}$*Il22*$^{-/-}$ mice engrafted with *Il22*$^{+/+}$or *Il22*$^{-/-}$ γδ T cells 24h postintrasplenic injection. n ≥ 7 mice per group. (O) Schematic overview of intrasplenic injection of MC38 GFP-labelled cells in *Tcrd*$^{GDL/GDL}$ *and Tcrd*$^{+/+}$ mice following DT (Diphtheria toxin) injection (DT injection in *Tcrd*$^{GDL/GDL}$ mice leads to γδ T cell depletion). n ≥ 7 mice per group. (P) Representative FACS plots and quantification of γδ T cells of *Tcrd*$^{GDL/GDL}$ *and Tcrd*$^{+/+}$ mice upon DT injection. (Q) Representative FACS plots and number of extravasated cancer cells from *Tcrd*$^{GDL/GDL}$ or *Tcrd*$^{+/+}$ mice 24h post intrasplenic injection. (R) Schematic overview of intrasplenic injection of MC38 cells for forced liver metastasis induction in *Ja18*$^{+/+}$ and *Ja18*$^{-/-}$ mice. (S) Representative pictures, number of macroscopic metastases in total liver and liver weight of *Ja18*$^{+/+}$ mice compared to *Ja18*$^{-/-}$ mice. n ≥ 6 mice per group. (T) Schematic overview of human liver metastasis. (U) Fresh specimen from resected liver metastasis and hematoxylin & eosin staining of perimetastatic and metastatic human liver. (V) Flow cytometry of perimetastatic and metastatic human liver and diagram showing the proportion of iNKT IL-22-producing cells in perimetastatic and metastatic human liver. Cells were isolated from fresh perimetastatic and metastatic liver tissue and analyzed using flow cytometry. n = 5 patients. Scale bar: 200μm. Data presented as mean ± SEM. ns>0.05; *:p<0.05; **:p≤0.01; ***:p≤0.001 as assessed by one-way ANOVA with Bonferroni post hoc tests (H, V) or Mann-Whitney U test (E, F, G, N, P, Q, S).

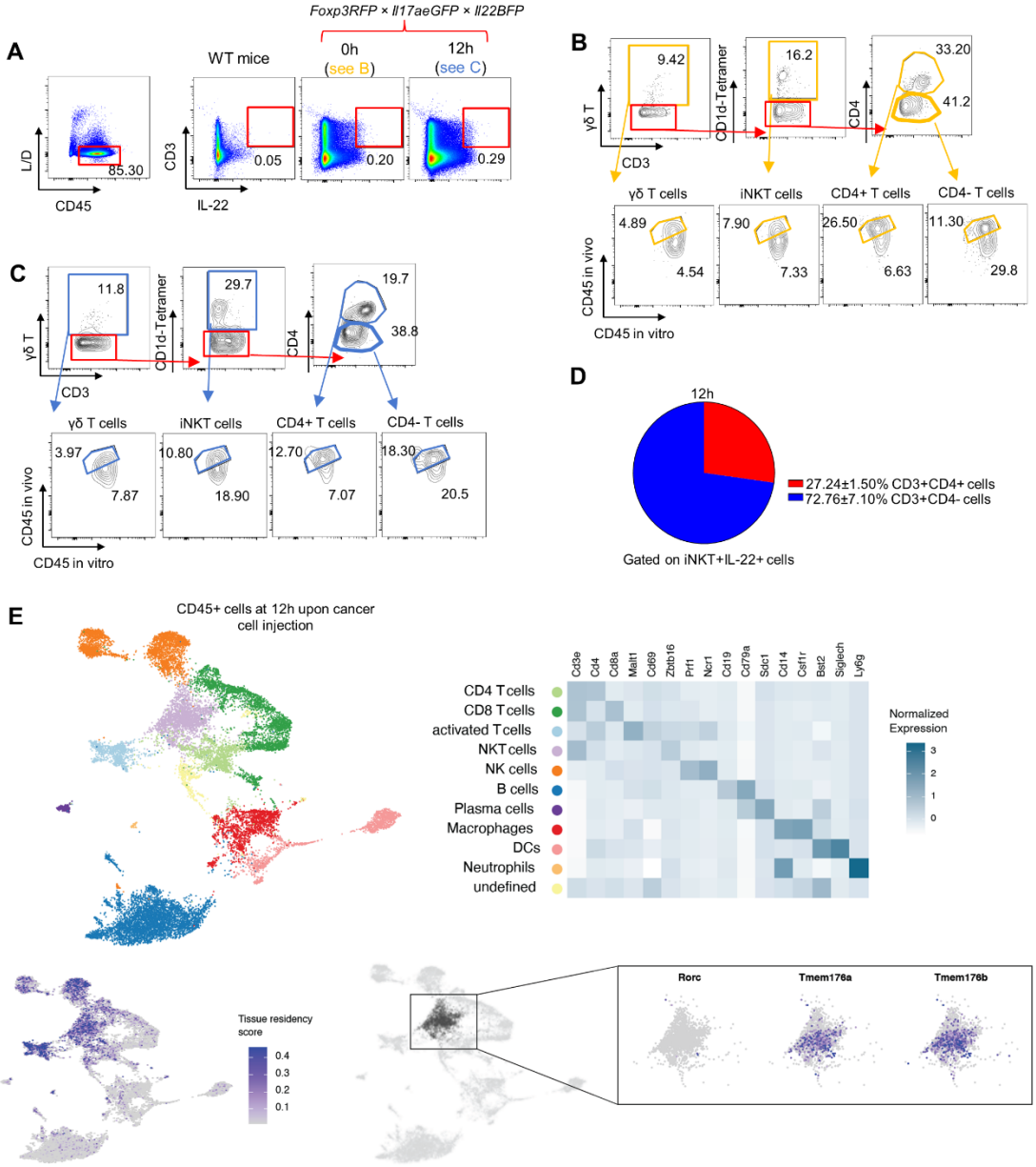
Foxp3RFP × Il17aeGFP × Il22BFP
A
WT mice
0h
(see B)
12h
(see C)
L/D
85.30
CD45
CD3
0.05
0.20
0.29
IL-22
B
9.42
16.2
33.20
41.2
γδ T
CD3
CD1d-Tetramer
CD4
γδ T cells
iNKT cells
CD4+ T cells
CD4- T cells
4.89
4.54
7.90
7.33
26.50
6.63
11.30
29.8
CD45 in vivo
CD45 in vitro
C
11.8
29.7
19.7
38.8
γδ T
CD3
CD1d-Tetramer
CD4
γδ T cells
iNKT cells
CD4+ T cells
CD4- T cells
3.97
7.87
10.80
18.90
12.70
7.07
18.30
20.5
CD45 in vivo
CD45 in vitro
D
12h
27.24±1.50% CD3+CD4+ cells
72.76±7.10% CD3+CD4- cells
Gated on iNKT+IL-22+ cells
E
CD45+ cells at 12h upon cancer cell injection
Cd3e
Cd4
Cd8a
Mait1
Cd69
Zbtb16
Prf1
Ncr1
Cd19
Cd79a
Sdc1
Cd14
Csf1r
Bst2
Siglech
Ly6g
CD4 T cells
CD8 T cells
activated T cells
NKT cells
NK cells
B cells
Plasma cells
Macrophages
DCs
Neutrophils
undefined
Normalized Expression
3
2
1
0
Tissue residency score
0.4
0.3
0.2
0.1
Rorc
Tmem176a
Tmem176b

Figure S7, related to Figure 7. IL-22 producing iNKT17 cells express tissue resident markers (A-C) Gating strategy used for Figure 7 C. (A) FACS plots showing the IL-22+ T cell populations in the livers of *Foxp3*^{RFP}*;Il17a*^{eGFP}*;Il22*^{BFP} mice 0h and 12h post MC38 cell injection compared to WT mice. (B,C) Representative FACS plots of the indicated fractions within the IL-22+ T cell population showing the percentage of infiltrating and circulating cells at 0h (B) and 12h (C). (D) The contribution of CD4+ and CD4- of iNKT+IL-22+ cells 12 hours upon intrasplenic cancer cell injection. (E) Cell clusters of identified CD45+ cells using single-cell sequencing in mouse livers 12 hours upon intrasplenic cancer cell injection, overlaid with tissue residency score and iNKT17 markers.

Supplementary table 1, related to the STAR method section: Taqman probes and primer sequences utilized for this study

gene	company	taqman probe/ primer name	sequence (5' → 3')
Il22-/-	Eurofins Genomics	IL22SU	TCA TCT GCT TGG TAC CAT GC
		IL22dRev	CAG AGA AAA TGG CAA GGC GG
		LacZ	GTC TGT CCT AGC TTC CTC ACT G
CD4Cre+	Eurofins Genomics	CD4Cre Mu	TTA GGG TGG GGC TCA GAA GG
		CD4Cre Co	AAC TTG CAC AGC TCA GAA TGC
		CD4Cre Wt	ACC TGA GAT TCC ACC AAA CTT GA
Il10GFP	Eurofins Genomics	GFP-3	AAG TCG TGC TGC TTC ATG TG
		GFP-5	ACG TAA ACG GCC ACA AGT TC
		IL10KOF	GTG TGT ATT GAG TCT GCT GGA C
		IL10KOR1	GTG TGG CCA GCC TTA GAA TAG
		IL10KOR2	GGT TGC CTT GAC CAT CGA TG
Foxp3RFP	Eurofins Genomics	FIR1	CAA AAC CAA GAA AAG GTG GGC
		FIR2	GGA ATG CTC GTC AAG AAG ACA GG
		FIR3	CAT CTT GGA GAG TCG GTG TG
Il22ra1-/-	Eurofins Genomics	CAS_R1_Term	TCG TGG TAT CGT TAT GCG CC
		IL22ra1_F	TCT GAT GCC CTC TTC TGC TG
		IL22ra1_R	TTG CTG GTC ACA GTC CAT CC
Il17Cre+	Eurofins Genomics	17AyfpF	CAA GTG CAC CCA GCA CCA GCT GAT C
		17AyfpRwt	CTT AGT GGG TTA GTT TCA TCA CAG C
		17AyfpCreR	GCA GCA GGG TGT AGG CAA TGC
Il22ra1flox/flox	Eurofins Genomics	IL22ra1_wt_R1	TGG GTC GGT TTG CAG ACT TG
		IL22ra1_wt_F1	GCC CTC TTC TGC TGT GTC TGA
Il22flox/flox	Eurofins Genomics	DNA460-40	CTC AGA CCT CTA CAG ACA ATC ATC
		DNA460-22	CAG CTG GCG GCC AAA GTC CC
AlbCre+	Eurofins Genomics	CreIA	GCA CTG ATT TCG ACC AGG TT
		CreIIB	CCC GGC AAA ACA GGT AGT TA
Cdh5Cre+	Eurofins Genomics	Cdh5-Cre Fw	GTC CAA TTT ACT GAC CGT ACA C
		Cdh5-Cre Rev	CTG TCA CTT GGT CGT GGC AGC
Rosa26YFP+	Eurofins Genomics	Rosa26 Seq1	AAA GTC GCT CTG AGT TGT TAT
		Rosa26 Seq2	GCG AAG AGT TTG TCC TCA ACC
		Rosa26 Seq3	GGA GCG GGA GAA ATG GAT ATG
Il17aeGFP	Eurofins Genomics	IL-17A KI sense	CAC CAG CGC TGT GTC AAT
		IL-17A KI anti sense	ACA AAC ACG AAG CAG TTT GG
		IL-17A KI IRES	ACC GGC CTT ATT CCA AGC
Il22BFP	Eurofins Genomics	TailWT22F	GTG CTC AGC AAG CAA ATG TC
		SiresFI	TAC GCT TGA GGA GAG CCA
		SHAGF	AAT GAT GGA CGT TAG CTT
		SHAGR	CCC GAC CAC ATG GGT TGA A
Apc15lox	Eurofins Genomics	int14loxF	AGG GTT ATT GAA TAT GAT CGG
		mInt14Apc-R4	AGC AGC AAA CTT ACT TTA CAG
		m14intApc-F3	AAC TTC TGA GTA TGA TGG AGG
	Eurofins Genomics	Kras22908	CTG CAT AGT ACG CTA TAC CCT GT

KrasG12D		Kras22907	TGT CTT TCC CCA GCA CAG T
		oIMR9592	GCA GGT CGA GGG ACC TAA TA
Il22tg8$^{(Tg)}$		Il22SV40_TG6/8	CCC ATT CAT CAG TTC CAT AG
		Il22CDNA_TG6/8	GAG TGG AGA GAG ATC AAG GCG ATT G
Il17aPe-Cy5	Eurofins Genomics	IL-17A KI sense	CAC CAG CGC TGT GTC AAT
		IL-17A KI anti sense	ACA AAC ACG AAG CAG TTT GG
		IL-17A KI IRES	ACC GGC CTT ATT CCA AGC
Rosa26 YFP	Eurofins Genomics	Rosa26 Seq1	AAA GTC GCT CTG AGT TGT TAT
		Rosa26 Seq2	GCG AAG AGT TTG TCC TCA ACC
		Rosa26 Seq3	GGA GCG GGA GAA ATG GAT ATG
Cd13-/-	Eurofins Genomics	CD13KO Forword	CAC CCC CAT CCC CCA TCC CTT AC
		CD13KO Reverse	GTG CCC ACG CCC TTG AAC CTT ACT T
		CD13KO IRESrev	ACAAACGCACACCGGCCTTATTCC
Rag1-/-	Eurofins Genomics	RagWF	GAG GTT CCG CTA CGA CTC TG
		RagR	CCG GAC AAG TTT TTC ATC GT
		RagMF	TGG ATG TGG AAT GTG TGC GAG
Ja18-/-	Eurofins Genomics	Ja18 Com	CTC AAA AGG CTG TGT AAT TGC T
		Ja18 Mut	CTT GGG GAT GTT TAC AGA GTA CC
		Ja18 WT	AGT CCC AGC TCC AAA ATG C
TcrdGDL/GDL	Eurofins Genomics	Delta FW	CTAGAAGAAAAGCAAAAGCCCTC
		Delta REV	CCTTCCTTTCGGTATTTTACTTTCA
		IRES REV	AAACGCACACCGGCCTTATT
Il22 cloning primer A	Eurofins Genomics	IL22 FW	ATG GCT GTC CTG CAG AAA TCT
		IL22 REV	TCA GAC GCA AGC ATT TCT CAG
Il22 cloning primer B	Eurofins Genomics	m_BglII_IL22	TCC GGA CTC AGA TCT ATG GCT GTC CTG CAG AAA TCT
		m_EcoRI _IL22	TCG ACT GCA GAA TTC TCA GAC GCA AGC ATT TCT CAG
Il22	Thermo Fisher Scientific	Mm01226722_g1	
Hprt	Thermo Fisher Scientific	Mm03024075_m1	
Anpep	Thermo Fisher Scientific	Mm00476227_m1	
Fgfr3	Thermo Fisher Scientific	Mm00433294_m1	
Epas1	Thermo Fisher Scientific	Mm00433294_m1	
Cdh5	Thermo Fisher Scientific	Mm00486938_m1	
Cxcl12	Thermo Fisher Scientific	Mm00445553_m1	
Nrp1	Thermo Fisher Scientific	Mm00435379_m1	
Angpt1	Thermo Fisher Scientific	Mm00456503_m1	
Plg	Thermo Fisher Scientific	Mm00447087_m1	
Cxcl16	Thermo Fisher Scientific	Mm00469712_m1	
Vegfa	Thermo Fisher Scientific	Mm00437306_m1	

Supplementary table 2, related to STAR method section: Cloning oligonucleotide sequences corresponding to shRNA and sgRNAs used in this study

Vector Backbone	Sigma mission #	Target of shRNA
pLKO.1-puro	SHC002	scrambled
pLKO.1-puro	TRCN0000050238	human *ANPEP* (CD13)
pLKO.1-puro	TRCN0000050239	human *ANPEP* (CD13)
pLKO.1-puro	TRCN0000050240	human *ANPEP* (CD13)
pLKO.1-puro	TRCN0000018482	human *ANPEP* (CD13)
pLKO.1-puro	TRCN0000025830	human *ANPEP* (CD13)
pLKO.1-puro	TRCN0000035991	human *ANPEP* (CD13)
pLKO.1-puro	TRCN0000065863	Mouse *Il22ra1*
pLKO.1-puro	TRCN0000065864	Mouse *Il22ra1*
pLKO.1-puro	TRCN0000065865	Mouse *Il22ra1*
pLKO.1-puro	TRCN0000065866	Mouse *Il22ra1*
pLKO.1-puro	TRCN0000065867	Mouse *Il22ra1*